THE JOURNAL OF PHYSICAL CHEMISTRY C

pubs.acs.org/JPCC Article

Photoactivated Refractive Index Anisotropy in Fluorescent Thiophene Derivatives

Adam Szukalski,* Karolina A. Haupa, Alina Adamow, Yohan Cheret, Raphael Hue, Abdelkrim El-Ghayoury,* Bouchta Sahraoui, Dario Pisignano, Jaroslaw Mysliwiec, and Andrea Camposeo*

Cite This: J. Phys. Chem. C 2020, 124, 25465−25472 Read Online

ACCESS | Metrics & More | Article Recommendations | Supporting Information

ABSTRACT: The optical control of anisotropy in materials is highly advantageous for many technological applications, including the real-time modulation of another light signal in photonic switches and sensors. Here, we introduce three thiophene derivatives with a donor−acceptor structure, which feature different positions of an electron-acceptor nitrile group, and both photoalignment and luminescence properties. Quantum chemical calculations highlight the presence of *trans*-forms stable at room temperature and metastable *cis*-isomers. Besides photoluminescence peaked at 440−460 nm and 0.4 ns lifetime, the three nonlinear optical chromophores exhibit photoinduced anisotropy of the refractive index closely depending on the specific molecular structure, with higher values of birefringence at lower driving signal being obtained for *ortho* substitution of the nitrile group. All-optical modulation of an external light beam at rates of hundreds of hertz is demonstrated in the fluorescent systems. This finding opens an interesting route to multispectral photonic switches embedded in the active layers of light-emitting devices.

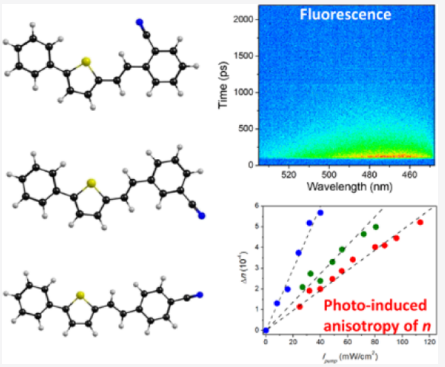

INTRODUCTION

The management of light propagation and of light−matter interaction benefits from the availability of materials whose physical properties can be controlled and varied in real time by means of external fields.[1−3] The properties of various optical materials and photonic devices such as absorption and fluorescence,[4] light-scattering,[5] optical gain and lasing,[6,7] and nonlinear optical (NLO) features[8,9] can be effectively modulated through electric and magnetic fields,[10,11] mechanical stretching,[12,13] temperature,[14] chemical interactions,[15,16] pressure,[17] or light.[18] Control achieved by light is especially interesting because the so-enabled, remote modulation of the properties of operating devices can be very fast and pushed at high spatial resolution by employing focused laser beams. For these reasons, light-responsive systems[19−22] are continuously expanding their fields of use, with recent examples including photoswitchable dual-color[23] and white light-emitting[24] nanoparticles, photochromic transparent wood for smart windows,[25] anticounterfeiting systems,[26] and UV sensors.[27] In this framework, achieving simultaneous optical control of light intensity and photon generation by compact, multifunctional systems would be of paramount importance, allowing passive and active light modulation to be potentially combined in super-resolution microscopy, optical computing and communications, multispectral sensing, diagnostics, and analytics.[23,28,29]

Molecules designed to optimize their NLO properties are highly relevant in this respect.[30] For instance, azobenzene derivatives were largely used as building blocks of light-responsive materials and surfaces.[31] Upon photoirradiation, *trans*-to-*cis* isomerization is activated in azobenzenes, which might lead to a neat photoalignment of chromophores along a given direction. Such anisotropy, in turn impacting optical absorption and refractive index, can be exploited for the passive modulation of a polarized light beam,[32] but it is not normally accompanied by light emission, that is, by passive/active multifunctionality. Other systems were reported, such as stilbene derivatives, that exhibit photon emission combined with NLO properties.[33,34] Second-harmonic generation (SHG) and light switching have been recently shown by pyrazoline derivatives, that is, *push−pull* donor−acceptor molecules based on the stilbene fragment.[35,36] Overall, these studies indicate that the SHG signal and photoinduced birefringence can be tailored by specific moieties and by varying the electron-donor and -acceptor units and their position.

Received: August 14, 2020
Revised: October 22, 2020
Published: November 9, 2020

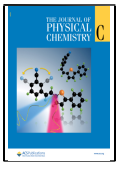

https://dx.doi.org/10.1021/acs.jpcc.0c07455
J. Phys. Chem. C 2020, 124, 25465−25472

Scheme 1. Scheme of the Synthetic Route of the Th-*o*CN, Th-*m*CN, and Th-*p*CN Derivatives

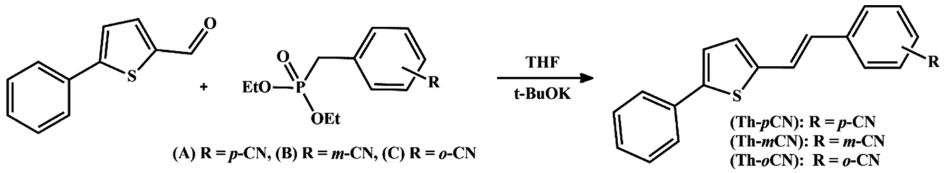

Here, we report on three new thiophene derivatives based on stilbene, designed as *push*−*pull* molecules with an aromatic electron-donor group and a nitrile acceptor group. The derivatives differ for the position of the acceptor unit with respect to an aromatic ring, close to the electron-acceptor region. Quantum chemical calculations determine the available isomers for each derivative and their structures. In addition to light emission with sub-nanosecond lifetime, the molecules are found to undergo photoisomerization upon optical pumping with a beam resonant with the absorption band, which is associated with molecular alignment and building-up of optical birefringence, allowing the intensity of polarized light to be switched at rates up to many hundreds of hertz. The investigated compounds display different magnitudes of their photoinduced birefringence, which provides a significant design pathway for enhancing optical switching and for combined passive/active light modulation by organic systems.

EXPERIMENTAL METHODS

Materials and Characterization Techniques. Commercially available reagents and solvents of analytical grade are used without any further purification. Diethylcyanobenzylphosophonate precursors (**A**−**C** in Scheme 1) are prepared following the Arbuzov reaction,[37] while the thiophene derivatives were obtained by the Horner−Wadsworth−Emmons reaction between phenylthiophenealdehyde and the phosphonate derivatives **A**−**C** (Scheme 1). All reactions are carried out under an inert nitrogen atmosphere. Nuclear magnetic resonance (NMR) spectra are measured by using a Bruker Avance DRX 300 spectrometer operating at 300 MHz for ^{1}H NMR and at 75 MHz for ^{13}C NMR. Mass spectra are collected with the Bruker Biflex-III apparatus.

Synthesis of Thiophene Derivatives and Film Preparation. For the synthesis of (*E*)-2-(2-(5-phenylthiophen-2-yl)vinyl)benzonitrile (Th-*o*CN), (*E*)-3-(2-(5-phenylthiophen-2-yl)vinyl)benzonitrile (Th-*m*CN), and (*E*)-4-(2-(5-phenylthiophen-2-yl)vinyl)benzonitrile (Th-*p*CN), a solution of potassium *tert*-butoxide (*t*-BuOK, 297 mg, 2.65 mmol) is added dropwise to a solution of diethylcyanobenzylphosphonate (268 mg, 1.06 mmol) in 20 mL of dry tetrahydrofuran (THF) in a three-necked flask under nitrogen (Scheme 1). The mixture is stirred for few minutes and, subsequently, a THF solution of 5-phenylthiophene-2-carbaldehyde (200 mg, 1.06 mmol) is added. The resulting mixture is stirred for one night and, after evaporation of THF, the resulting product is dissolved in dichloromethane (DCM) and washed with an aqueous NaCl solution. The organic phase is collected, and the solvent was left to evaporate. The resulting product undergoes silica gel chromatography column using petroleum ether/DCM 3:1 (v/v) followed by petroleum ether/DCM 1:1 (v/v) as the eluent to afford the resulting compound. The reaction yield and the results of the NMR characterization of the Th-*x*CN (*x* = *o*, *m* and *p*) compounds are reported in the Supporting Information (Figures S1−S4).

Th-*x*CN-doped poly(methyl methacrylate) (PMMA, Sigma-Aldrich) films are drop-cast on silica glass plates from DCM solutions (2% dry w/w dopant/polymer ratio). After mixing, stirring for 24 h, and drop-casting, films are formed under solvent vapors during the next 24 h, and their thickness (4−5 μm) is measured in different areas of the samples using a DektakXT (Bruker) profilometer.

Computational Analysis. Quantum-chemical calculations are performed using the Gaussian 09 program.[38] Geometrical optimization and harmonic vibrational analysis are carried out by density functional theory with the B3LYP functional.[39] The standard Dunning's correlation-consistent basis set augmented with diffuse functions (aug-cc-pVDZ) is used.[40] The nature of the stationary points is checked by the calculation of the vibrational frequency, obtained for all minimum energies and found to have no imaginary values. The obtained relative energies include zero-point vibrational energy corrections. The abundances of the found conformers at room temperature are calculated according to the Boltzmann distribution.

Absorption and Time-Resolved Fluorescence. Absorption and fluorescence spectra of Th-*x*CN in PMMA are measured by the Jasco V-550 UV−vis spectrophotometer and the Varian Cary Eclipse fluorescence spectrometer, respectively. The investigation of the photoluminescence (PL) lifetime is carried out by a femtosecond laser (Legend, Coherent) and a streak-camera (C10910, Hamamatsu) coupled to a spectrograph (Acton SpectraPro SP-2300, Princeton Instruments). More specifically, the second harmonic (λ = 400 nm) of the output beam of the femtosecond laser system (wavelength: 800 nm, pulse duration: 90 fs, repetition rate = 1 kHz) is focused on the sample surface by a lens (focal distance, 100 mm), while the emitted light is collected by the same lens in a backscattering geometry and coupled to the monochromator by a second lens (focal distance, 100 mm). The absolute fluorescence quantum yield (Φ_F) is measured by an integrating sphere (LabSphere).[41] To this aim, the samples are optically pumped by a 375 nm continuous wave (cw) diode laser (L6Cc, OXXIUS).

Optically Induced Birefringence. For the investigation of the optical birefringence property that is induced optically, a cw pump−probe experimental setup is used, similar to the one typically utilized for the investigation of the optical Kerr effect.[42] This method relies on the measurement of the variation of the polarization direction of a probe beam (λ_{probe} = 638 nm, i.e., in the Th-*x*CN transparency region), which is induced by a pump laser beam (λ_{pump} = 405 nm, i.e., in the absorption band of the used molecules), as schematized in Figure S5 in the Supporting Information. To this aim, two diode lasers of the L6Cc system (OXXIUS) are used. To maximize the photoinduced birefringence effect, the pumping beam polarization direction is rotated by 45° with respect to the polarization direction of the incident probe beam by means of a half waveplate. A cross-polarizer configuration is used for the probe beam. More specifically, the probe beam is linearly

https://dx.doi.org/10.1021/acs.jpcc.0c07455
J. Phys. Chem. C 2020, 124, 25465−25472

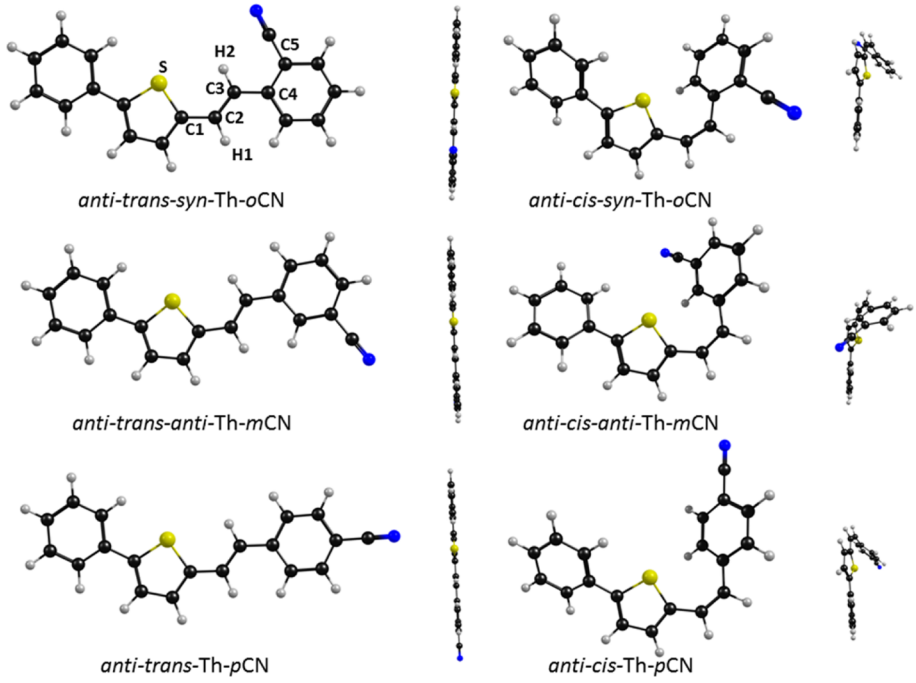

Figure 1. Optimized geometries of the most stable conformers of *trans*- and *cis*-Th-*o*CN, Th-*m*CN, and Th-*p*CN calculated with the B3LYP/aug-cc-pVDZ method. In-plane view (left) and out-of-plane view (right) are shown for each conformer by considering the plane containing the thiophene group.

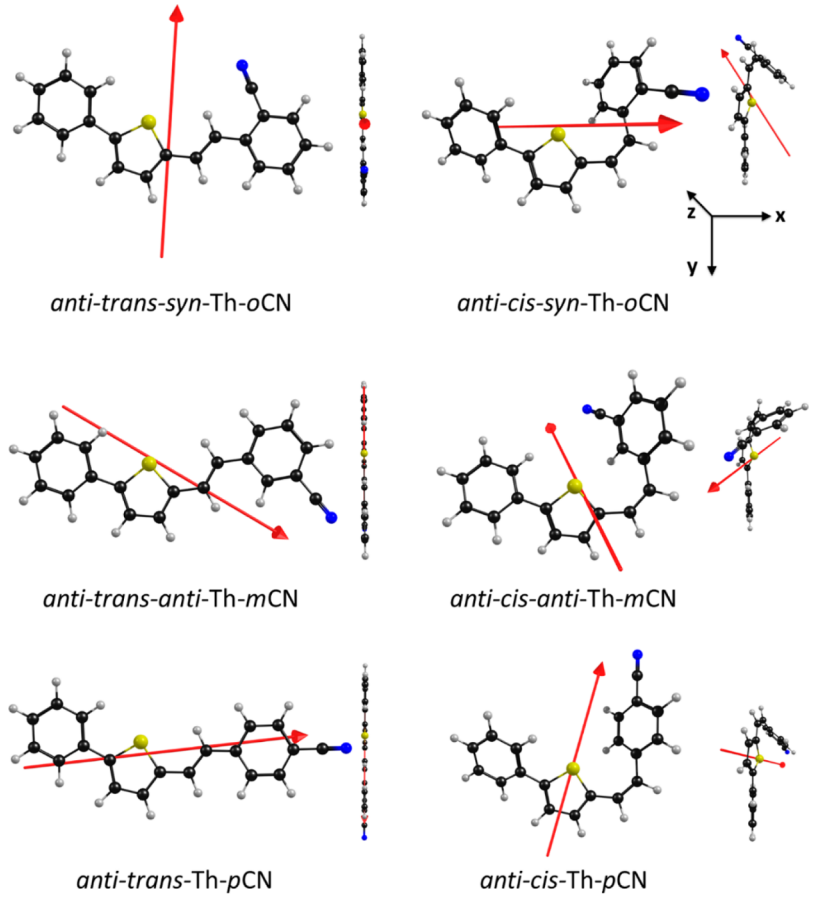

Figure 2. Orientation of dipole moment vectors for the most stable conformers of *trans*- and *cis*-Th-*o*CN, Th-*m*CN, and Th-*p*CN. In-plane view (left) and out-of-plane view (right) are shown for each conformer.

https://dx.doi.org/10.1021/acs.jpcc.0c07455
J. Phys. Chem. C 2020, 124, 25465−25472

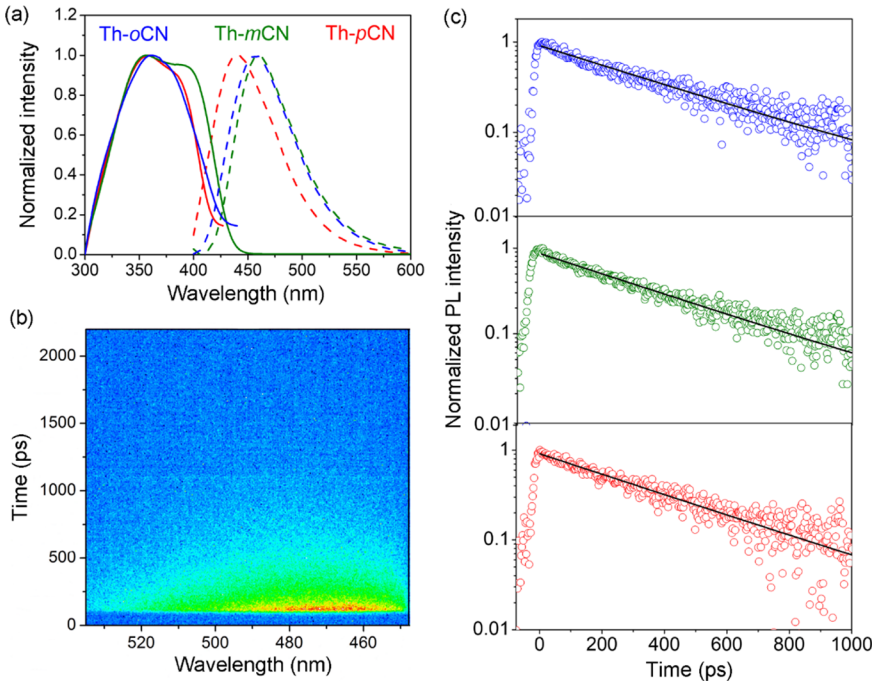

Figure 3. Th-*x*CNs in PMMA. (a) Absorption (solid line) and PL (dashed line) spectra. (b) Exemplary 2-dimensional PL intensity map showing the spectrally and time-resolved emission of Th-*o*CN. (c) PL temporal decay for Th-*o*CN (blue dots), Th-*m*CN (green dots), and Th-*p*CN (red dots). The black continuous lines are a fit to the data by a monoexponential curve.

polarized by a first polarizer placed between the light source and the sample, whereas a second polarizer (analyzer) with the axis perpendicular to the first one is placed on the path of the probe beam that is transmitted by a sample. The intensity of so transmitted light is measured by a Si photodiode located behind the analyzer (Figure S5). In such a configuration, the intensity of the probe beam transmitted by an optically isotropic material placed between the polarizer and the analyzer is zero. In contrast, any anisotropy induced in the refractive index of the Th-*x*CN samples will cause a rotation of the polarization direction of the probe beam passing through them, namely, a nonzero transmission through the analyzer. The magnitude of the photoinduced optical anisotropy can be calculated by the expression[35,36,43]

$$I_{\text{probe}}^{\text{T}} = I_{\text{probe}}^{0} \sin^2\left(\frac{\pi d \Delta n(I_{\text{pump}})}{\lambda_{\text{probe}}}\right) \quad (1)$$

where I_{probe}^{0} and $I_{\text{probe}}^{\text{T}}$ are the incident and transmitted intensities of the probe beam, respectively, d is the sample thickness, and $\Delta n(I_{\text{pump}})$ is the pump intensity (I_{pump})-dependent anisotropy of the refractive index, namely, the difference of the refractive index for light polarized parallel and perpendicular to the direction of polarization of the pump. Two temporal regimes can be typically considered in the experiments: one is related to the steady-state photoalignment of molecules upon optical pumping. This can be evaluated by the stationary amplitude of the probe signal detected by the photodiode with the pump beam switched on. Indeed, thanks to the many photoinduced conformational changes of the active molecules (typically *trans*−*cis*−*trans* transformations), it is possible to photoalign a significant population of the initially isotropic molecules, with an associated increase of Δn typically occurring on timescales (τ_{on}) of seconds or minutes in solid-state systems.[35,36,43] Such optically induced birefringence typically vanishes on timescales (τ_{off}) comparable to τ_{on} upon switching off the pumping beam.[44] Another interesting regime is associated with variations of the pump intensity much faster than τ_{on}, but sufficiently long to observe the effect of conformational changes, which occur typically in sub-millisecond timescale.[35,36,45] This regime, which is appealing for fast light modulation, can be inspected by modulating the pump intensity with a mechanical chopper (Figure S5) and measuring the corresponding variation of the transmitted probe intensity.

RESULTS AND DISCUSSION

Quantum Chemical Calculations. The systematic scan of the potential energy surface allows six minima for Th-*o*CN and Th-*m*CN and four minima for Th-*p*CN to be found. The optimized *trans*- and *cis*-conformers of Th-*o*CN, Th-*m*CN, and Th-*p*CN are shown in Figure 1, whereas the structures of conformers with higher energy are shown in Figure S6. The relative energies, Gibbs free enthalpies, and abundance at the room temperature of all the structures found for the three compounds are summarized in Table S1 in the Supporting Information. *Trans*-isomers are lower in energy and have a

Table 1. Summary of the Photophysical Properties of Th-*x*CNs in PMMA[a]

	$\lambda_{\text{max}}^{\text{abs}}$ (nm)	$\lambda_{\text{max}}^{\text{PL}}$ (nm)	$\Delta\lambda_{\text{SS}}$ (nm)	Φ_{F} (%)	τ_{PL} (ns)	k_{r} (ns^{-1})	k_{nr} (ns^{-1})
Th-*o*CN	361	457	96	6	0.4	0.15	2.4
Th-*m*CN	357	460	103	5	0.4	0.13	2.4
Th-*p*CN	358	440	82	5	0.4	0.13	2.4

[a] $\lambda_{\text{max}}^{\text{abs}}$ and $\lambda_{\text{max}}^{\text{PL}}$: peak wavelength of the absorption and PL spectra, respectively, $\Delta\lambda_{\text{SS}}$: Stokes shift, Φ_{F}: PL quantum yield, τ_{PL}: PL lifetime, $k_{\text{r}} = \Phi_{\text{F}}/\tau_{\text{PL}}$ and $k_{\text{nr}} = (1 - \Phi_{\text{F}})/\tau_{\text{PL}}$: radiative and nonradiative decay rates, respectively.

https://dx.doi.org/10.1021/acs.jpcc.0c07455
J. Phys. Chem. C 2020, 124, 25465−25472

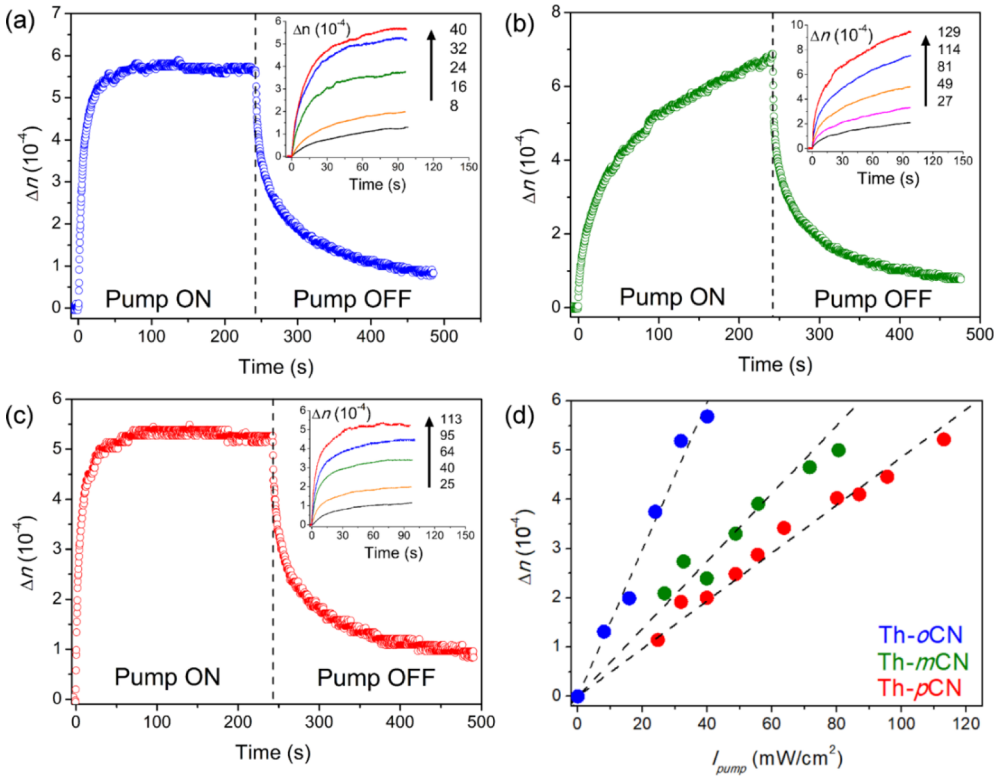

Figure 4. (a–c) Temporal evolution of the photoinduced birefringence, Δn, for the and Th-*o*CN (a), Th-*m*CN (b), and Th-*p*CN (c), respectively, upon switching on and off the pump beam. Pumping intensities: 40 (a), 96 (b), 113 mW cm^{-2} (c). The insets show the increase of Δn for various intensities of the pump beam (reported in mW cm^{-2}). (d) Dependence of Δn on the incident intensity of the pump beam, I_{pump} (data collected after 250 s with pump on).

planar configuration. Only these isomers are predicted to contribute to the population at ambient temperature. In order to rationalize the structure of the conformers, the energies associated with the torsions along S–C1–C2–C3, H1–C2–C3–H2, and H2–C3–C4–C5 (atom notation shown in Figure 1) bonds are calculated (Figure S7). The estimated energy barrier for *trans* → *cis* isomerization is about 80 kcal mol^{-1}, and it is almost comparable for all the investigated molecules, as can be appreciated by scanning the angle H1–C2–C3–H2 (Figure S7b,e,h). Furthermore, the possibility of rotation along S–C1–C2–C3 and H2–C3–C4–C5 bonds gives conformational flexibility to *trans*-Th-*x*CN, leading to *syn*- and *anti*-conformers. Scan of the S–C1–C2–C3 bond shows that the rotation of the thiophene ring has a small energy barrier (~10 kcal mol^{-1}, Figure S7a,d,g). Rotation of the Ph–CN group along the H2–C3–C4–C5 bond has a significantly higher barrier (~40 kcal mol^{-1}, Figure S7c,f,i). Rotation barriers appear to be independent from the position of the –CN group (Figure S7). For Th-*o*CN, the *anti–trans–syn* conformer is identified as the global minimum with a calculated abundance of 72%. For Th-*m*CN, *anti–trans–anti* and *anti–trans–syn* isomers are very close in energy, and their abundance at room temperature is comparable, that is, 45 and 42%, respectively. Substitution in the *para* position in Th-*p*CN limits the number of conformers to four. The *anti–trans* conformer was found as the conformer with minimum energy, with 89% contribution to the population at room temperature.

The calculated values of the dipole moment for all the optimized conformers are also summarized in Table S1. The orientation of dipole moments for the most stable *trans*- and *cis*-conformers is shown in Figure 2. The different position of the electron-acceptor unit impacts the spatial orientation of the dipole moment. For the *trans*-form of Th-*m*CN and Th-*p*CN, the dipole moment is in the plane containing the thiophene group, along the direction from the donor to the acceptor unit. *trans*-Th-*o*CN displays a significantly different orientation of the dipole moment vector that is almost orthogonal to the donor-to-acceptor unit direction (Figure 2). In addition, the calculated dipole moments reported in Table S1 evidence an impact of the different position of the electron-acceptor unit, the *trans*-Th-*p*CN featuring the dipole with the highest magnitude. Overall, these features are expected to determine different properties at the solid state, where both steric and electronic effects (including dipolar interactions) influence the final packing of the molecules,[46,47] with a possibly more closed packed stacking for the *para* derivative (see also the different color of the powders shown in Figure S1).

In the case of nonplanar *cis*-conformers, the vector of dipole moment is oriented from the donor to the acceptor, out-of-the-plane containing the thiophene group.

Spectroscopy. The absorption and fluorescence spectra of Th-*x*CNs in PMMA are shown in Figure 3a. All the systems show a double-band absorption spectrum, with a maximum at ~360 nm and another one at ~395 nm (for Th-*m*CN and Th-*p*CN) and at ~410 nm (for Th-*o*CN), respectively. The PL measurements show broad (full width at half-maximum, in the range 65–70 nm) and featureless bands peaked at 440 nm (for Th-*p*CN) and at 457–460 nm (for Th-*o*CN and Th-*m*CN), respectively. All the Th-*x*CNs in PMMA show PL quantum yields stable at 5–6%, and monoexponential temporal decay of the PL with a lifetime (τ_{PL}) of about 0.4 ns (Figure 3b,c and

https://dx.doi.org/10.1021/acs.jpcc.0c07455
J. Phys. Chem. C 2020, 124, 25465–25472

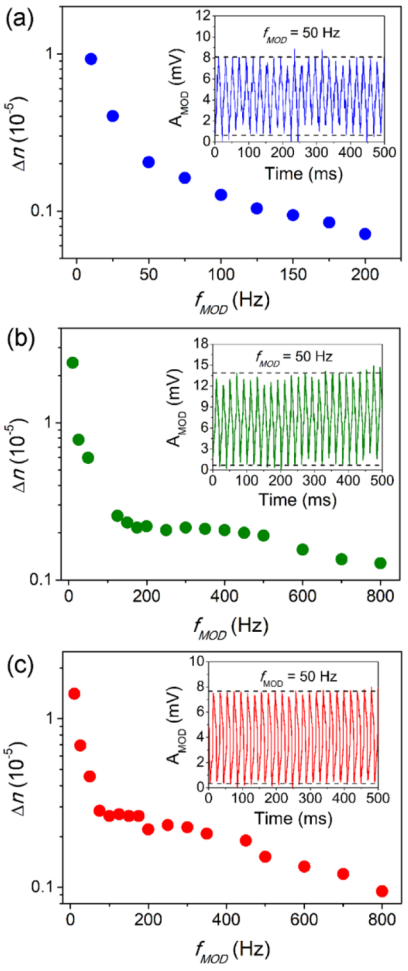

Figure 5. Amplitude of the modulated birefringence vs the modulation frequency (f_{MOD}) of the driving, pump beam for Th-*o*CN (a), Th-*m*CN (b), and Th-*p*CN (c), respectively. Insets: exemplary temporal evolution of the optically modulated probe signal, measured at f_{MOD} = 50 Hz and I_{pump} = 40 mW cm^{-2} for Th-*o*CN (a), I_{pump} = 95 mW cm^{-2} for Th-*m*CN (b) and Th-*p*CN (c), respectively.

Table 1), compatible with fast modulation of the spontaneous emission (up to GHz rates).

Photoinduced Birefringence and Optical Switching. The build-up of photoinduced birefringence, Δn, upon light irradiation and its relaxation in dark conditions are shown in Figure 4a–c. For all the Th-*x*CNs, we find an increase of the photoinduced birefringence over time with the pump laser active, followed by a decrease in absence of pump light, with the first trend being related to the photoalignment of the guest molecules in the PMMA matrix following *trans*-to-*cis* photoisomerization, while the latter being related to the thermal relaxation of the metastable *cis*-isomers back to the *trans*-ones that are stable at room temperature (Table S1). The photoalignment properties are related to various factors, including the molecular readjustments accompanying the *trans*–*cis*–*trans* isomerization (Figure 1), which are tightly dependent on the polymer host. Here, Th-*m*CN displays a slower build-up of the anisotropy of the refractive index (Figure 4b), which does not reach saturation in the investigated time interval of 250 s. Instead, Th-*p*CN (Figure 4c) clearly shows a saturation of the birefringence at Δn = 5.2 × 10^{-4} upon optical pumping at I_{pump} ∼ 113 mW cm^{-2}. Saturation occurs in about 100 s, almost independently of the used pump (inset of Figure 4c). For the sake of comparison, we recall that this timescale is 2 times faster than that in which Δn saturation is reached in a host/guest system incorporating a thiophene derivative with a nitro group as an electron-acceptor unit [(*E*)-2-(4-nitrostyryl)-5-phenylthiophene, Th-*p*NO$_2$].[48]

Th-*o*CN exhibits an even more effective kinetics of the refractive index anisotropy build-up (Figure 4a), with Δn ∼5.7 × 10^{-4} achieved by lower pumping intensity (40 mW cm^{-2}). In the framework of third-order NLO phenomena,[43] a linear behavior with slope n_2 is expected for the dependence of the photoinduced birefringence on the pump intensity, $\Delta n = n_2 \times I_{pump}$. This is shown in Figure 4d for the three molecules here investigated, showing that Th-*o*CN allows given Δn values to be obtained by pump beam intensities about 2 and 3 times lower than and Th-*m*CN and Th-*p*CN, respectively (see Table S2) and much lower with respect to previously reported Th-*p*NO$_2$, for which a Δn ∼ 1.52 × 10^{-4} was measured at I_{pump} = 840 mW cm^{-2}.[48] This result is highly relevant in view of realizing photoresponsive systems to control with low optical intensity.

Finally, the modulation of the intensity of the probe beam by optical control is evidenced in Figure 5. The temporal stability and repeatability of the intensity modulation of the probe beam are highlighted in the insets of Figure 5a–c and in Figure S8. The decrease of the amplitude of the probe beam modulation follows the decrease of the time interval during which the active molecules are illuminated by the pump laser light, which corresponds to the time interval, in which cyclic conversion between *trans* and *cis* conformational states, and the associated increase of optical anisotropy of the refractive index occur. Interestingly, a modulation corresponding to Δn of the order of 10^{-6} is still found at about 800 Hz, which is interesting for many applications requiring intensity and/or phase modulation of light beams, such as additive manufacturing, imaging, optical communication, and computation.[49,50] In this respect, it is worth mentioning that the modulation of the probe beam is promoted together with the modulation of the PL intensity, whose lifetime is much shorter than the timescale (∼ms) here used to control the photoinduced birefringence. This would enable concomitant and intrinsically synchronous all-optical switching of light at multiple wavelengths, namely, the wavelengths of the probe beams passing through the Th-*x*CN samples (638 nm) and of the sample PL (i.e., 440–460 nm).

CONCLUSIONS

In summary, three light-responsive thiophene compounds based on the stilbene group are introduced, varying the position of their electron-acceptor unit. Quantum chemical calculations allowed the most stable conformers to be identified and their geometrical configuration and properties to be determined. The Th-*x*CNs show blue PL with a sub-nanosecond (0.4 ns) lifetime. The investigation of the third-order NLO properties evidences effective photoalignment in all the Th-*x*CN on a timescale of 10^2 s, with an associated increase of the refractive index anisotropy. Such photoinduced birefringence is exploited for achieving all-optical control on a polarized light beam, and it appears to be more easily induced in Th-*o*CN which makes it particularly appealing to be used with low driving intensities. The possibility of concomitant all-optical modulation of the light emitted by the photoactive systems and of external light beams makes these compounds highly promising for all those applications where synchronous

https://dx.doi.org/10.1021/acs.jpcc.0c07455
J. Phys. Chem. C 2020, 124, 25465–25472

modulation of multiple light signals is required such as multidimensional analytical and imaging systems and photonic networks.

■ ASSOCIATED CONTENT

Supporting Information

The Supporting Information is available free of charge at https://pubs.acs.org/doi/10.1021/acs.jpcc.0c07455.

NMR spectra and data, structures of conformers with higher energies, calculated energy increase of the conformers upon scanning the torsion angles, additional data about all-optical modulation of light intensity, and experimental setup used for characterization of photo-induced anisotropy of the refractive index (PDF)

■ AUTHOR INFORMATION

Corresponding Authors

Adam Szukalski − *NEST, Istituto Nanoscienze-CNR and Scuola Normale Superiore, I-56127 Pisa, Italy; Faculty of Chemistry, Wroclaw University of Science and Technology, 50-370 Wroclaw, Poland;* orcid.org/0000-0003-1062-0812; Email: adam.szukalski@pwr.edu.pl

Abdelkrim El-Ghayoury − *MOLTECH-Anjou, UMR 6200, CNRS, Université Angers, 49045 Angers Cedex, France;* orcid.org/0000-0003-2787-3859; Email: abdelkrim.elghayoury@univ-angers.fr

Andrea Camposeo − *NEST, Istituto Nanoscienze-CNR and Scuola Normale Superiore, I-56127 Pisa, Italy;* orcid.org/0000-0002-3533-7389; Email: andrea.camposeo@nano.cnr.it

Authors

Karolina A. Haupa − *Department of Applied Chemistry and Institute of Molecular Science, National Chiao Tung University, 30010 Hsinchu, Taiwan; Institute of Physical Chemistry, Karlsruhe Institute of Technology, D-76131 Karlsruhe, Germany;* orcid.org/0000-0002-6604-4730

Alina Adamow − *NEST, Istituto Nanoscienze-CNR and Scuola Normale Superiore, I-56127 Pisa, Italy; Faculty of Chemistry, Wroclaw University of Science and Technology, 50-370 Wroclaw, Poland*

Yohan Cheret − *MOLTECH-Anjou, UMR 6200, CNRS, Université Angers, 49045 Angers Cedex, France*

Raphael Hue − *MOLTECH-Anjou, UMR 6200, CNRS, Université Angers, 49045 Angers Cedex, France*

Bouchta Sahraoui − *MOLTECH-Anjou, UMR 6200, CNRS, Université Angers, 49045 Angers Cedex, France*

Dario Pisignano − *NEST, Istituto Nanoscienze-CNR and Scuola Normale Superiore, I-56127 Pisa, Italy; Dipartimento di Fisica, Università di Pisa, I-56127 Pisa, Italy;* orcid.org/0000-0003-3758-5199

Jaroslaw Mysliwiec − *Faculty of Chemistry, Wroclaw University of Science and Technology, 50-370 Wroclaw, Poland*

Complete contact information is available at: https://pubs.acs.org/10.1021/acs.jpcc.0c07455

Notes

The authors declare no competing financial interest.

■ ACKNOWLEDGMENTS

The research leading to these results has received funding from the European Research Council under the European Union's Horizon 2020 Research and Innovation Programme (grant agreement no. 682157, "*x*PRINT"), from the Italian Ministry of University and Research PRIN 201795SBA3 project, and from the National Science Center, Poland (2018/31/B/ST8/02832). Calculations have been carried out in Wroclaw Centre for Networking and Supercomputing (http://www.wcss.wroc.pl), grant no. 409. K.A.H. is a recipient of an Alexander von Humboldt fellowship.

■ REFERENCES

(1) Li, Z.; Yin, Y. Stimuli-Responsive Optical Nanomaterials. *Adv. Mater.* **2019**, *31*, 1807061.

(2) van Heeswijk, E. P. A.; Kragt, A. J. J.; Grossiord, N.; Schenning, A. P. H. J. Environmentally Responsive Photonic Polymers. *Chem. Commun.* **2019**, *55*, 2880.

(3) Isapour, G.; Lattuada, M. Bioinspired Stimuli-Responsive Color-Changing Systems. *Adv. Mater.* **2018**, *30*, 1707069.

(4) Berkovic, G.; Krongauz, V.; Weiss, V. Spiropyrans and Spirooxazines for Memories and Switches. *Chem. Rev.* **2000**, *100*, 1741−1754.

(5) Samai, S.; Qian, Z.; Ling, J.; Guye, K. N.; Ginger, D. S. Optical Properties of Reconfigurable Polymer/Silver Nanoprism Hybrids: Tunable Color and Infrared Scattering Contrast. *ACS Appl. Mater. Interfaces* **2018**, *10*, 8976−8984.

(6) Wiersma, D. S.; Cavalieri, S. A temperature-tunable random laser. *Nature* **2001**, *414*, 708−709.

(7) Zhang, W.; Yan, Y.; Gu, J.; Yao, J.; Zhao, Y. S. Low-Threshold Wavelength-Switchable Organic Nanowire Lasers Based on Excited-State Intramolecular Proton Transfer. *Angew. Chem., Int. Ed.* **2015**, *54*, 7125.

(8) Koos, C.; Vorreau, P.; Vallaitis, T.; Dumon, P.; Bogaerts, W.; Baets, R.; Esembeson, B.; Biaggio, I.; Michinobu, T.; Diederich, F.; et al. All-Optical High-Speed Signal Processing with Silicon−Organic Hybrid Slot Waveguides. *Nat. Photonics* **2009**, *3*, 216−219.

(9) Tao, K.; Wu, Z.; Han, S.; Zhang, J.; Ji, C.; Wang, Y.; Zhang, W.; Luo, J.; Sun, Z. Switchable Behaviors of Quadratic Nonlinear Optical Properties Originating from Bi-Step Phase Transitions in a Molecule-Based Crystal. *J. Mater. Chem. C* **2018**, *6*, 4150−4155.

(10) Adamow, A.; Sznitko, L.; Chrzumnicka, E.; Stachera, J.; Szukalski, A.; Martynski, T.; Mysliwiec, J. The Ultra-Photostable and Electrically Modulated Stimulated Emission in Perylene-Based Dye Doped Liquid Crystal. *Sci. Rep.* **2019**, *9*, 2143−2148.

(11) Zhang, X.; Li, Z.; Feng, J.; Yang, F.; Wu, C.; Fan, Q.; Zhou, S.; Yin, Y. Dynamic Tuning of Optical Transmittance of 1D Colloidal Assemblies of Magnetic Nanostructures. *Adv. Intell. Syst.* **2019**, *1*, 1900099.

(12) Sagara, Y.; Kato, T. Mechanically Induced Luminescence Changes in Molecular Assemblies. *Nat. Chem.* **2009**, *1*, 605−610.

(13) Park, W.; Lee, J.-B. Mechanically Tunable Photonic Crystal Structure. *Appl. Phys. Lett.* **2004**, *85*, 4845−4847.

(14) Ke, Y.; Zhou, C.; Zhou, Y.; Wang, S.; Chan, S. H.; Long, Y. Emerging Thermal-Responsive Materials and Integrated Techniques Targeting the Energy-Efficient Smart Window Application. *Adv. Funct. Mater.* **2018**, *28*, 1800113.

(15) Davis, D. A.; Hamilton, A.; Yang, J.; Cremar, L. D.; Van Gough, D.; Potisek, S. L.; Ong, M. T.; Braun, P. V.; Martínez, T. J.; White, S. R.; et al. Force-Induced Activation of Covalent Bonds in Mechanoresponsive Polymeric Materials. *Nature* **2009**, *459*, 68−72.

(16) Yan, X.; Wang, F.; Zheng, B.; Huang, F. Stimuli-Responsive Supramolecular Polymeric Materials. *Chem. Soc. Rev.* **2012**, *41*, 6042−6065.

(17) Wang, Y.; Tan, X.; Zhang, Y.-M.; Zhu, S.; Zhang, I.; Yu, B.; Wang, K.; Yang, B.; Li, M.; Zou, B.; et al. Dynamic Behavior of

Molecular Switches in Crystal under Pressure and Its Reflection on Tactile Sensing. *J. Am. Chem. Soc.* **2015**, *137*, 931−939.
(18) Nie, H.; Self, J. L.; Kuenstler, A. S.; Hayward, R. C.; Read de Alaniz, J. Multiaddressable Photochromic Architectures: from Molecules to Materials. *Adv. Opt. Mater.* **2019**, *7*, 1900224.
(19) Delaire, J. A.; Nakatani, K. Linear and Nonlinear Optical Properties of Photochromic Molecules and Materials. *Chem. Rev.* **2000**, *100*, 1817−1846.
(20) Klajn, R. Spiropyran-Based Dynamic Materials. *Chem. Soc. Rev.* **2014**, *43*, 148.
(21) Wang, L.; Li, Q. Photochromism into Nanosystems: Towards Lighting up the Future Nanoworld. *Chem. Soc. Rev.* **2018**, *47*, 1044.
(22) Zhang, X.; Hou, L.; Samorì, P. Coupling Carbon Nanomaterials with Photochromic Molecules for the Generation of Optically Responsive Materials. *Nat. Commun.* **2016**, *7*, 11118.
(23) Kim, D.; Jeong, K.; Kwon, J. E.; Park, H.; Lee, S.; Kim, S.; Park, S. Y. Dual-Color Fluorescent Nanoparticles Showing Perfect Color-Specific Photoswitching for Bioimaging and Super-Resolution Microscopy. *Nat. Commun.* **2019**, *10*, 3089.
(24) Wang, H.; Zhang, P.; Krishnan, B. P.; Yu, M.; Liu, J.; Xue, M.; Chen, S.; Zeng, R.; Cui, J.; Chen, J. Switchable Single Fluorescent Polymeric Nanoparticles for Stable White-Light Generation. *J. Mater. Chem. C* **2018**, *6*, 9897.
(25) Wang, L.; Liu, Y.; Zhan, X.; Luo, D.; Sun, X. Photochromic Transparent Wood for Photo-Switchable Smart Window Applications. *J. Mater. Chem. C* **2019**, *7*, 8649.
(26) Abdollahi, A.; Sahandi-Zangabad, K.; Roghani-Mamaqani, H. Rewritable Anticounterfeiting Polymer Inks Based on Functionalized Stimuli-Responsive Latex Particles Containing Spiropyran Photoswitches: Reversible Photopatterning and Security Marking. *ACS Appl. Mater. Interfaces* **2018**, *10*, 39279−39292.
(27) Liu, L.; Ren, Y.; Pan, J.; Liu, Z.; Wu, B.; Yan, F. Printable UV-Light Sensor for Human Eye Protection. *ACS Appl. Mater. Interfaces* **2020**, *12*, 1495−1503.
(28) Wu, Y.; Guo, Z.; Zhu, W.-H.; Wan, W.; Zhang, J.; Li, W.; Li, X.; Tian, H.; Li, A. D. Q. Photoswitching Between Black and Colourless Spectra Exhibits Resettable Spatiotemporal Logic. *Mater. Horiz.* **2016**, *3*, 124.
(29) Li, J.; Bisoyi, H. K.; Tian, J.; Guo, J.; Li, Q. Optically Rewritable Transparent Liquid Crystal Displays Enabled by Light-Driven Chiral Fluorescent Molecular Switches. *Adv. Mater.* **2019**, *31*, 1807751.
(30) Yerushalmi, R.; Scherz, A.; van der Boom, M. E.; Kraatz, H.-B. Stimuli Responsive Materials: New Avenues Toward Smart Organic Devices. *J. Mater. Chem.* **2005**, *15*, 4480−4487.
(31) Sobolewska, A.; Bartkiewicz, S.; Miniewicz, A.; Schab-Balcerzak, E. Polarization Dependence of Holographic Grating Recording in Azobenzene-Functionalized Polymers Monitored by Visible and Infrared Light. *J. Phys. Chem. B* **2010**, *114*, 9751−9760.
(32) Miniewicz, A.; Kochalska, A.; Mysliwiec, J.; Samoc, A.; Samoc, M.; Grote, J. G. Deoxyribonucleic Acid-Based Photochromic Material for Fast Dynamic Holography. *Appl. Phys. Lett.* **2007**, *91*, 041118.
(33) Dobryakov, A. L.; Quick, M.; Richter, C.; Knie, C.; Ioffe, I. N.; Granovsky, A. A.; Mahrwald, R.; Ernsting, N. P.; Kovalenko, S. A. Photoisomerization pathways and Raman activity of 1,1′-difluorostilbene. *J. Chem. Phys.* **2017**, *146*, 044501−044518.
(34) He, T.; Wang, Y.; Tian, X.; Gao, Y.; Zhao, X.; Grimsdale, A. C.; Lin, X.; Sun, H. An Organic Dye with Very Large Stokes-Shift and Broad Tunability of Fluorescence: Potential Two-Photon Probe for Bioimaging and Ultra-Sensitive Solid-State Gas Sensor. *Appl. Phys. Lett.* **2016**, *108*, 011901−011905.
(35) Szukalski, A.; Haupa, K.; Miniewicz, A.; Mysliwiec, J. Photoinduced Birefringence in PMMA Polymer Doped with Photoisomerizable Pyrazoline Derivative. *J. Phys. Chem. C* **2015**, *119*, 10007−10014.
(36) Szukalski, A.; Miniewicz, A.; Haupa, K.; Przybyl, B.; Janczak, J.; Sobolewski, A. L.; Mysliwiec, J. Photo-Physical Transformations in Pyrazoline Derivative Based Systems. *J. Phys. Chem. C* **2016**, *120*, 14813−14819.
(37) Wadsworth, W. S.; Emmons, W. D. The Utility of Phosphonate Carbanions in Olefin Synthesis. *J. Am. Chem. Soc.* **1961**, *83*, 1733−1738.
(38) Frisch, M. J.; Trucks, G. W.; Schlegel, H. B.; Scuseria, G. E.; Robb, M. A.; Cheeseman, J. R.; Scalmani, G.; Barone, V.; Mennucci, B.; Petersson, G. A.; Nakatsuji, H.; et al. *Gaussian 09*, Revision A.1; Gaussian, Inc.: Wallingford CT, 2009.
(39) Boys, S. F.; Bernardi, F. The Calculation of Small Molecular Interactions by the Differences of Separate Total Energies. Some Procedures With Reduced Errors. *Mol. Phys.* **1970**, *19*, 553−566.
(40) Dunning, T. H. Gaussian basis sets for use in correlated molecular calculations. I. The Atoms Boron through Neon and Hydrogen. *J. Chem. Phys.* **1989**, *90*, 1007−1023.
(41) de Mello, J. C.; Wittmann, H. F.; Friend, R. H. An Improved Experimental Determination of External Photoluminescence Quantum Efficiency. *Adv. Mater.* **1997**, *9*, 230.
(42) Szukalski, A.; Moffa, M.; Camposeo, A.; Pisignano, D.; Mysliwiec, J. All-Optical Switching in Dye-Doped DNA Nanofibers. *J. Mater. Chem. C* **2019**, *7*, 170−176.
(43) Boyd, R. W. *Nonlinear Optics*, 3rd ed.; Academic Press: New York, 2008.
(44) Miniewicz, A.; Girones, J.; Karpinski, P.; Mossety-Leszczak, B.; Galina, H.; Dutkiewicz, M. Photochromic and Nonlinear Optical Properties of Azo-Functionalized POSS Nanoparticles Dispersed in Nematic Liquid Crystals. *J. Mater. Chem. C* **2014**, *2*, 432−440.
(45) Poprawa-Smoluch, M.; Baggerman, J.; Zhang, H.; Maas, H. P. A.; De Cola, L.; Brouwer, A. M. Photoisomerization of Disperse Red 1 Studied with Transient Absorption Spectroscopy and Quantum Chemical Calculations. *J. Phys. Chem. A* **2006**, *110*, 11926−11937.
(46) Yao, Z.-F.; Wang, J.-Y.; Pei, J. Control of $\pi-\pi$ Stacking via Crystal Engineering in Organic Conjugated Small Molecule Crystals. *Cryst. Growth Des.* **2018**, *18*, 7−15.
(47) Takacs, C. J.; Sun, Y.; Welch, G. C.; Perez, L. A.; Liu, X.; Wen, W.; Bazan, G. C.; Heeger, A. J. Solar Cell Efficiency, Self-Assembly, and Dipole-Dipole Interactions of Isomorphic Narrow-Band-Gap Molecules. *J. Am. Chem. Soc.* **2012**, *134*, 16597−16606.
(48) Szukalski, A.; Ayadi, A.; Haupa, K.; El-Ghayoury, A.; Sahraoui, B.; Mysliwiec, J. All-Optical Switching and Two-States Light-Controlled Coherent-Incoherent Random Lasing in a Thiophene-Based Donor-Acceptor System. *ChemPhysChem* **2018**, *19*, 1605−1616.
(49) Bléger, D.; Hecht, S. Visible-Light-Activated Molecular Switches. *Angew. Chem., Int. Ed.* **2015**, *54*, 11338.
(50) Hoffmann, M.; Papadopoulos, I. N.; Judkewitz, B. Kilohertz Binary Phase Modulator for Pulsed Laser Sources Using a Digital Micromirror Device. *Opt. Lett.* **2018**, *43*, 22.

https://dx.doi.org/10.1021/acs.jpcc.0c07455
J. Phys. Chem. C 2020, 124, 25465−25472